






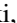











Structure of $^{126,128}\text{Xe}$ studied in Coulomb excitation measurements

S. Kisiov ^{1,*} C. Y. Wu ¹ J. Henderson ² A. Gade ^{3,4} K. Kaneko ⁵ Y. Sun ⁶ N. Shimizu ⁷ T. Mizusaki ⁸ D. Rhodes ^{3,4,†}
S. Biswas ³ A. Chester ³ M. Devlin ⁹ P. Farris ^{3,4} A. M. Hill ^{3,4} J. Li ³ E. Rubino ³ and D. Weisshaar ³

¹Lawrence Livermore National Laboratory, Livermore, California 94550, USA

²Department of Physics, University of Surrey, Guildford, Surrey GU2 7XH, United Kingdom

³National Superconducting Cyclotron Laboratory, Michigan State University, East Lansing, Michigan 48824, USA

⁴Department of Physics and Astronomy, Michigan State University, East Lansing, Michigan 48824, USA

⁵Department of Physics, Kyushu Sangyo University, Fukuoka 813-8503, Japan

⁶School of Physics and Astronomy, Shanghai Jiao Tong University, Shanghai 200240, China

⁷Center for Computational Sciences, University of Tsukuba, 1-1-1, Tennodai Tsukuba, Ibaraki 305-8577, Japan

⁸Institute of Natural Sciences, Senshu University, Tokyo 101-8425, Japan

⁹Los Alamos National Laboratory, Los Alamos, New Mexico 87545, USA



(Received 5 July 2022; accepted 2 September 2022; published 19 September 2022)

The electromagnetic properties of $^{126,128}\text{Xe}$ were studied in subbarrier Coulomb excitation measurements performed at the National Superconducting Cyclotron Laboratory Re-accelerator facility, ReA3, at Michigan State University (MSU). ^{126}Xe and ^{128}Xe nuclei were accelerated to 3.74 and 3.81 MeV/nucleon, respectively, and were impinged on ^{196}Pt and ^{208}Pb targets. The γ rays deexciting the populated low-lying states were detected in coincidence with the scattered nuclei using the JANUS setup. Transition and diagonal matrix elements for low-lying states and transitions in $^{126,128}\text{Xe}$ were extracted from the experimental data using the GOSIA and GOSIA2 codes. The experimental results were compared with the theoretical calculations by the microscopic shell model and the Davydov-Filippov γ -rigid rotor model. The calculated results from the newly established shell model (called the PMMU model), which is based on the advanced Hartree-Fock Bogoliubov plus generator coordinate method (HFB + gcm) for a large model space, agree well with the measurements in both nuclei, except for the second 2^+ state. Interpretation for the experimentally determined nearly vanishing electric-quadrupole moment of this state remains a challenge for theory.

DOI: [10.1103/PhysRevC.106.034311](https://doi.org/10.1103/PhysRevC.106.034311)

I. INTRODUCTION

Atomic nuclei are among the most fascinating quantum many-body systems and exhibit a rich variety of shapes. Most nuclei are often assumed to have a quadrupole-deformed, axially symmetric shape in the ground state. However, in some regions in the nuclear chart axial symmetry in the quadrupole deformation breaks down and a triaxial description is required to characterize the properties of these nuclei. With just four protons above the shell closure at $Z = 50$, the stable, even- A isotopes $^{126,128}\text{Xe}$ provide a good opportunity to study the emergence of nuclear deformation and collectivity. Experimental properties of many nuclei in this mass region indicate a

transitional character, as might be expected as one moves from nominally spherical Sn nuclei towards the midshell region. The ratio of the excitation energies of the first 4^+ and 2^+ excited states ($R_{4/2}$) in the even- A Xe nuclei, in particular, increases towards the midshell between $N = 50$ and $N = 82$. Nevertheless, it does not reach values above $R_{4/2} \approx 2.5$ which are typical for γ -soft nuclei [1].

For nuclei exhibiting nonaxial symmetric shapes, one must also consider the roles of γ -soft and γ -rigid deformation. There are two extreme phenomenological models that describe the triaxiality: a γ -rigid rotor model of Davydov and Filippov (DF) [2] and a γ -soft model of Wilets and Jean (WJ) [3]. The O(6) dynamical symmetry of the interacting boson model (IBM) is strongly related to the WJ picture of γ softness. For the ground-state bands, both the DF and WJ models give rise to similar level energies and $E2$ transition strengths and, therefore, it is hard to delineate the two conceptually different collective modes. It was suggested by Otsuka and Sugita [4] that the two descriptions are equivalent. Nevertheless, there has been continuing effort in searching distinguishing features between the DF and WJ pictures. For example, Zamfir and Casten [5] and Bhat *et al.* [6] demonstrated that the phase of the odd-even staggering

*kisiov1@llnl.gov

†Present address: TRIUMF, Vancouver, British Columbia V6T 2A3, Canada.

Published by the American Physical Society under the terms of the [Creative Commons Attribution 4.0 International](https://creativecommons.org/licenses/by/4.0/) license. Further distribution of this work must maintain attribution to the author(s) and the published article's title, journal citation, and DOI.

(i.e., the staggering of the odd- and even-spin levels) of the γ -vibrational bands could shed light on the nature of triaxiality. A more stringent test is to examine the entire set of quadrupole matrix elements, not only the transition ones but also the diagonal ones, for the ground-state bands as well as other low-lying collective states. The most relevant collective state is the bandhead of the excited level sequence starting with 2^+ , traditionally known as the γ -vibrational state.

Recent theoretical and experimental works study the even- A Xe isotopes in the context of a possible critical point in the shape transition from spherical to γ -soft, O(6)-like nuclei. The increase of the excitation energies in the ground-state band within the O(6) limit is faster compared with the vibrational nuclei but slower than the typical values for rotational structures. Although the energy gaps in the ground-state band can give an indication to recognize possible O(6)-like structures, a real probe to test the relationship to this dynamical symmetry are electromagnetic properties of the nuclei [7]. A particularly important feature within the γ -soft framework is the vanishing of the quadrupole moments.

The experimental characteristics of the light stable Xe isotopes exhibit properties similar to those expected for the O(6) limit, but notable differences from some O(6) transition strengths were observed [8,9]. Also, while $E(5)$ critical-point behavior for the shape transition from a spherical vibrator to a triaxially soft rotor was proposed for the structure of ^{128}Xe [10], other investigations [9] suggest that ^{130}Xe is the most likely $E(5)$ candidate among the Xe isotopes. Central to all of these arguments is the role of triaxiality, which presently available data are insufficient to quantify. Thus, more experimental studies are needed in order to make firm statements about the relation to these dynamical symmetries.

In particular, very few experimental data are available for the quadrupole moments of excited states in the even- A Xe isotopes. The importance of such information in O(6) or γ -unstable nuclei is emphasized by the example of ^{128}Xe in Ref. [11]. Although a lot of experimentally known features of this nucleus can be related to the structure predicted by the O(6) symmetry, it is evident that different theoretical approaches [11,12] can reproduce the ^{128}Xe level scheme similarly well and yet predict very different quadrupole moments. The consequence is that level schemes are not a sensitive enough probe, and $B(E2)$ values can provide more detailed comparisons, but quadrupole moments are the most stringent test of theoretical models [11].

Different Coulomb excitation measurements were previously performed in the even- A Xe isotopes [8,9,13–15] but definitive conclusions about the diagonal matrix elements were still outstanding.

The present work is focused on the structure of the low-lying excited states in $^{126,128}\text{Xe}$. Experimental details are outlined in Sec. II while the data analysis procedures and results are presented in Sec. III. The newly determined values are compared with theoretical model calculations in Sec. IV. The comparison with the large-scale shell model (called the PMMU model) results is one of the first extensive applications of this newly developed shell model in such heavy and complex nuclei.

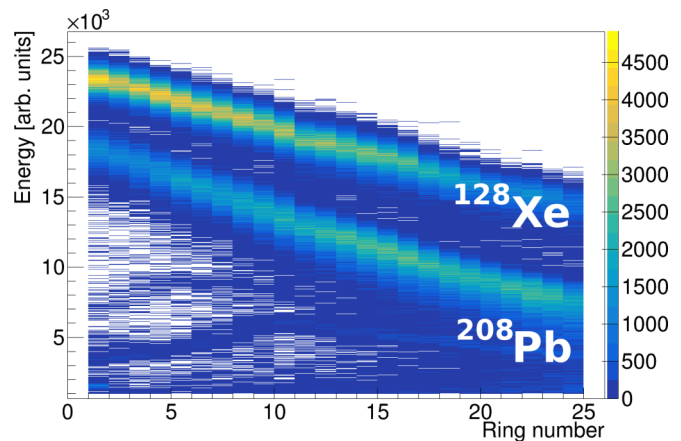


FIG. 1. Particle identification of the ^{128}Xe projectile and ^{208}Pb target nuclei in the forward Si detector. The kinematic lines for the ^{128}Xe projectile (upper locus) and ^{208}Pb target (lower locus) represent the particle energies when scattering at different angles. The angle increases with ring number.

II. EXPERIMENTAL DETAILS

Electromagnetic properties of $^{126,128}\text{Xe}$ were studied in a subbarrier Coulomb excitation experiment performed at the National Superconducting Cyclotron Laboratory (NSCL), Michigan State University (MSU). $^{126,128}\text{Xe}$ from an ion source were injected into NSCL's electron-beam ion trap [16] where they were charge bred to 43^+ , 44^+ , respectively, and injected into the ReA linear accelerator. The $^{126,128}\text{Xe}$ nuclei were delivered at energies of 3.74 and 3.81 MeV/nucleon, respectively, having the so-called “safe” Coulomb-excitation criterion [17] in consideration. The Xe nuclei were both impinged on a ^{208}Pb target with a thickness of 0.92 mg/cm^2 and a ^{196}Pt target with a thickness of 1.59 mg/cm^2 . The average beam intensity was $\approx 3 \times 10^5$ pps for the ^{128}Xe and $\approx 2 \times 10^5$ pps for the ^{126}Xe runs.

The Joint Array for Nuclear Structure (JANUS) [18] experimental setup was used in the measurements, allowing for a coincident detection of both the scattered nuclei and the γ rays following the Coulomb excitation. The detector configuration consists of a pair of segmented Micron S3-type double-sided Si detectors (Bambino2) and the Segmented Ge Array (SeGA) [19]. The Si detector pair includes two 24-ring detectors which cover the angular ranges 23.8° – 53.8° and 133.8° – 161.3° with respect to the beam axis. SeGA is comprised of sixteen 32-fold segmented high-purity germanium detectors with cylindrical crystals positioned around the target chamber in a barrel geometry [18,20].

III. DATA ANALYSIS AND EXPERIMENTAL RESULTS

The experimental data were sorted and analyzed using the GRUTINIZER code [21], based on the ROOT framework [22]. Particle identification and selection of the scattered projectile and recoiling target nuclei was determined by their different kinematic properties as measured in the Si detectors (as shown in Fig. 1). The Si data were subdivided into four

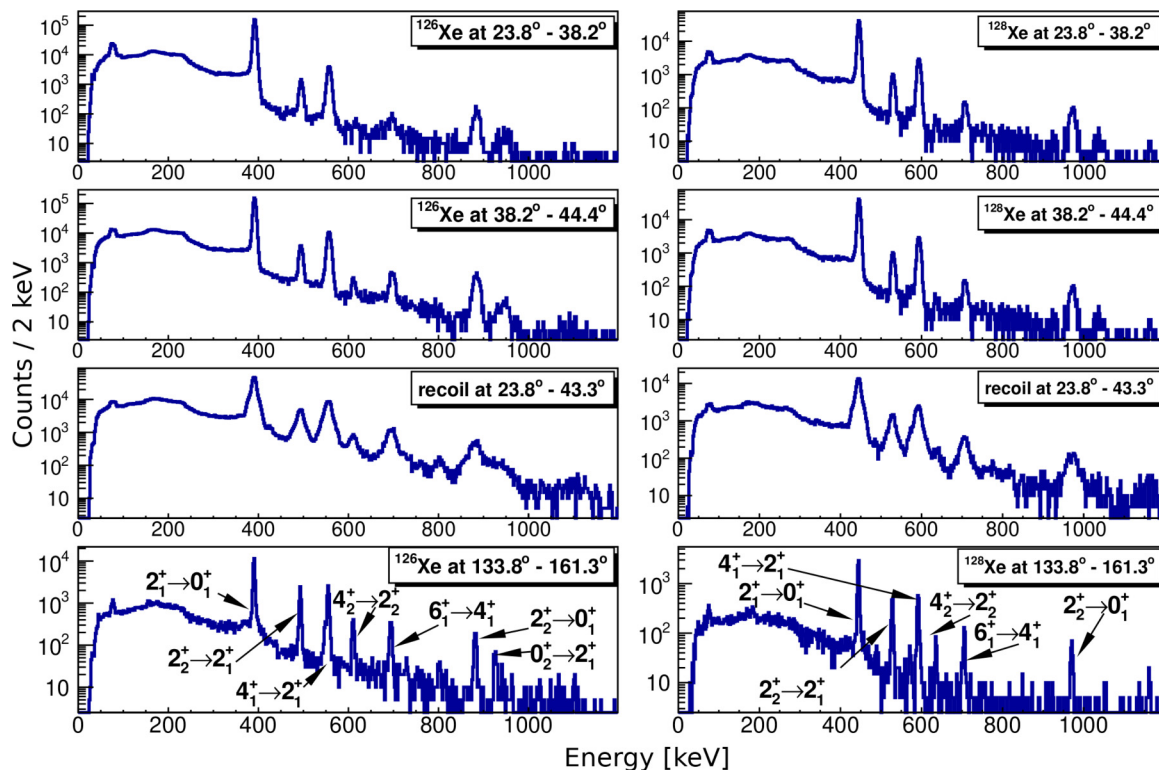


FIG. 2. Doppler-corrected γ -ray spectra in coincidence with Xe nuclei registered in the double-sided Si detector for runs with a target of ^{208}Pb and a beam of (left) ^{126}Xe and (right) ^{128}Xe . The γ -ray transitions representing the deexcitation of the populated states in the nuclei are labeled in the bottom spectra (Xe nuclei detected at backwards angles).

angular ranges—one with events in which $^{126,128}\text{Xe}$ nuclei were detected in the backwards Si detector (133.8° – 161.3° with respect to the beam axis), two of them include events with $^{126,128}\text{Xe}$ nuclei detected in the forward Si detector (23.8° – 38.2° and 38.2° – 44.4° , respectively), and the last data set includes events in which target nuclei were detected in the forward Si detector in the range of 23.8° – 43.3° .

Doppler-corrected γ -ray energy spectra of ^{126}Xe and ^{128}Xe are shown in Fig. 2 while partial level schemes of both nuclei are presented in Figs. 3. and 4. The γ -ray transitions observed in the present measurements are highlighted in red.

Experimental γ -ray yields coincident with the subdivided Si-detector data were efficiency corrected for use in the Coulomb-excitation analysis. They were compared with yields calculated using the semiclassical Coulomb excitation code, GOSIA, in order to extract electromagnetic matrix elements [23,24].

The $\langle 2_1^+ \| E2 \| 0_1^+ \rangle$ matrix elements in $^{126,128}\text{Xe}$ were first determined from the ^{196}Pt target datasets, following a combined GOSIA + GOSIA2 analysis procedure [25,26], as outlined in Ref. [27]. The excited states and transitions shown in Figs. 3 and 4 were used in the analysis process. The matrix elements of transitions which were not observed in the present experiment were set to values known from previously performed measurements, along with variations within the cited 1σ uncertainty limits [1].

The final experimental set of electromagnetic matrix elements for both nuclei was determined after χ^2 minimizations

in a standard GOSIA analysis including experimental γ -ray yields from both target datasets for each nucleus.

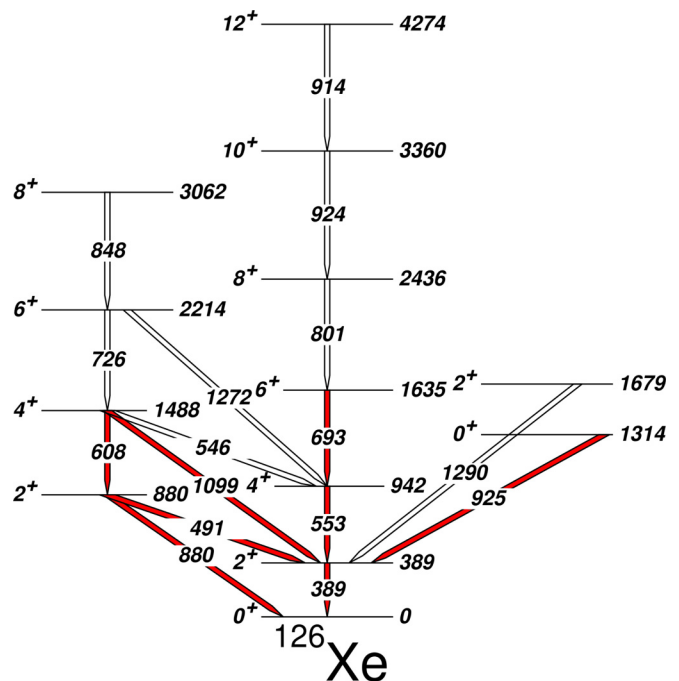


FIG. 3. A partial level scheme of ^{126}Xe . The data were taken from Ref. [28]. Transitions which were observed in the current work are highlighted in red.

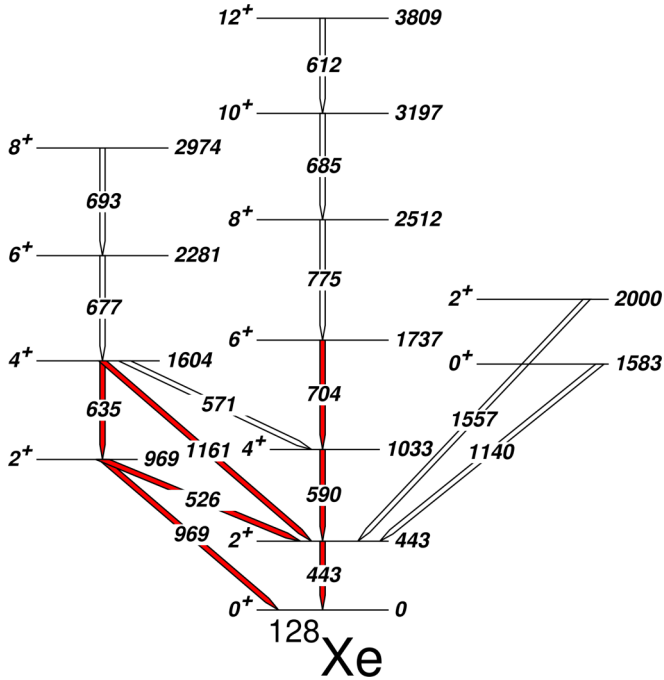


FIG. 4. A partial level scheme of ^{128}Xe . The data were taken from Ref. [29]. Transitions which were observed in the current work are highlighted in red.

The minimizations were performed on the basis of the γ -ray yields measured in the present experiment and previously available data [1,29–32]. Known branching ratios and mixing ratios (see Table I) were taken into account in the GOSIA + GOSIA2 iterative procedure conducted with the ^{196}Pt target datasets. Additional lifetimes literature information (shown in Table I) for states in ^{128}Xe was also used during the final GOSIA minimization. A value of $\tau = 26.8$ (3) ps for the lifetime of the first 2^+ state in ^{128}Xe was used as a data point during this data analysis step. It was determined as a weighted average of two out of several lifetime results reported in Ref. [30]. This value is consistent with the $\langle 2^+ \parallel E2 \parallel 0^+ \rangle$ matrix element obtained in the present work using the GOSIA + GOSIA2 iterative procedure for analysis of the ^{196}Pt target dataset [corresponding to $\tau = 26.6$ (9) ps].

The determined transition and diagonal matrix elements were used to calculate $B(E2)$ values and quadrupole moments. Transition probabilities from the analysis of the datasets are listed in Table II, along with comparison to results from previous measurements. Quadrupole moments of the 2^+_1 , 4^+_1 , and 2^+_2 states were calculated from the experimental diagonal matrix elements and are presented in Table III. The signs of all matrix elements measured in the present work were chosen as positive by convention, except for the diagonal matrix elements and the relative signs of the interband transitions which are measurable physical observables [34]. The low quadrupole moments of the second 2^+ states are notable, deviating from the expected theoretical values listed in Table III.

Along with results from measurements in previous works, the transition and the diagonal elements in Tables II and III are also compared with theoretical calculations performed by

TABLE I. Experimental values for branching ratios (BR), $E2/M1$ mixing ratios (δ), and lifetimes (τ) in $^{126,128}\text{Xe}$ known prior to the current work. The data for the branching and mixing ratios were taken from Refs. [1,29,31] while the data for the lifetimes of states in ^{128}Xe were taken from Refs. [30,32]. These values were used in the GOSIA minimization procedures to determine diagonal and transition matrix elements in $^{126,128}\text{Xe}$.

^{126}Xe				
J_i^π	J_f^π	E_γ [keV]	BR	δ
2^+_2	2^+_1	491	1	+9.1 (+43 –23)
2^+_2	0^+_1	880	0.2541 (19)	
4^+_2	2^+_2	608	1	
4^+_2	2^+_1	1099	0.211 (3)	
4^+_2	4^+_1	546	0.504 (5)	+3.0 (+10 –9)
^{128}Xe				
J_i^π	J_f^π	E_γ [keV]	BR	δ
2^+_2	2^+_1	526	1	+4.4 (7)
2^+_2	0^+_1	969	0.268 (5)	
4^+_2	2^+_2	635	1	
4^+_2	2^+_1	1161	0.361 (10)	
4^+_2	4^+_1	571	0.772 (19)	+1.9 (+3 –5)
J^π	E [keV]		τ [ps]	
2^+_1	443		26.8 (3)	
4^+_1	1033		4.8 (2)	
6^+_1	1737		1.8 (2)	
2^+_2	969		8.7 (5)	
4^+_2	1604		3.5 (2)	

the DF model [2] and the recently developed shell model [35]. The asymmetric rotor-model values were deduced within the approach outlined in Ref. [2], with the triaxiality parameters γ determined from the experimental transition matrix elements of the second 2^+ excited states in $^{126,128}\text{Xe}$. The results for the asymmetric rotor calculations were normalized with respect to the experimental values of the transition matrix elements of the first-excited state in each nucleus. The details about the theoretical calculations and outline for the shell model are presented in Sec. IV.

The uncertainties of the transition matrix elements, and therefore the $B(E2)$ values, were obtained by taking into account all possible correlations between the matrix elements [23]. The majority of the new results agree with the known literature data within a 1σ uncertainty interval. A notable difference is observed between the measured $B(E2; 2^+_1 \rightarrow 0^+_1)$ value in ^{126}Xe and the previously known data.

A different approach was used to determine the uncertainties of the diagonal matrix elements and quadrupole moments. For a range of fixed diagonal matrix elements of a given state of interest, GOSIA χ^2 minimizations were performed where all other matrix elements involving the decays of the 2^+_1 , 4^+_1 , and 2^+_2 states were allowed to vary. This leads to a χ^2 distribution for the diagonal matrix elements, allowing the 1σ uncertainty to be determined by the simple $\chi^2 + 1$ criterion [33].

A visualization of the results and the uncertainty estimation procedure for the diagonal matrix elements of the first

TABLE II. Transition matrix elements and $B(E2)$ values in $^{126,128}\text{Xe}$ determined in the present work. A comparison to results from previously performed measurements and theoretical calculations is presented. Known literature values of BR , δ , and τ (as noted in Table I) were used along with the present experimental data to determine the matrix elements.

^{126}Xe								
J_i^π	J_f^π	$\langle J_i^\pi E2 J_f^\pi \rangle_{\text{expt}}$ [eb]	$B(E2)_{\text{expt}}$ [W.u.]	$\langle J_i^\pi E2 J_f^\pi \rangle_{\text{PMMU}}$ [eb]	$B(E2)_{\text{PMMU}}$ [W.u.]	$B(E2)_{\text{DF}}$ [W.u.]	$B(E2)^{\text{a}}$ [W.u.]	
2_1^+	0_1^+	1.03 (4)	56 (5)	0.99	51	56	41.0 (13) ^b	
4_1^+	2_1^+	1.48 (4)	65.1 (34)	1.63	77	79	71.0 (67)	
6_1^+	4_1^+	2.07 (9)	88 (8)	2.13	91	99	84 (11)	
2_2^+	2_1^+	1.00 (4)	54 (4)	0.96	48	56	43.2 (26)	
2_2^+	0_1^+	0.119 (9)	0.75 (11)	0.125	0.82	1.86	0.63 (7)	
4_2^+	2_2^+	0.97 (6)	27.6 (34)	1.31	50	26	36.1 (42)	
0_2^+	2_1^+	0.12 (4)	3.9 (29)	0.15	5.8		5.9 (9)	
^{128}Xe								
J_i^π	J_f^π	$\langle J_i^\pi E2 J_f^\pi \rangle_{\text{expt}}$ [eb]	$B(E2)_{\text{expt}}$ [W.u.]	$\langle J_i^\pi E2 J_f^\pi \rangle_{\text{PMMU}}$ [eb]	$B(E2)_{\text{PMMU}}$ [W.u.]	$B(E2)_{\text{DF}}$ [W.u.]	$B(E2)^{\text{c}} \& B(E2)^{\text{d}}$ [W.u.]	[W.u.]
2_1^+	0_1^+	0.940 (15)	46.1 (15)	0.92	44	46.1	47 (5)	42.6 (64) ^e
4_1^+	2_1^+	1.38 (4)	55.4 (32)	1.51	66	65	60 (6)	63.5 (52)
6_1^+	4_1^+	1.95 (12)	76 (10)	2.00	80	82	79 (8)	106 (13)
2_2^+	2_1^+	0.92 (4)	44 (4)	1.02	54	46	49 (5)	50.1 (97)
2_2^+	0_1^+	0.105 (8)	0.58 (9)	0.068	0.24	1.56	0.63 (5)	0.65 (8)
4_2^+	2_2^+					21	29 (5)	29.6 (29)

^aFrom Ref. [8].

^bThe study in Ref. [8] uses a value from Ref. [31].

^cFrom Ref. [13].

^dFrom Ref. [9].

^eThe study in Ref. [9] uses a value from Ref. [36].

and second 2^+ states in ^{126}Xe is presented in Fig. 5. The values determined using this approach are consistent with the full correlated uncertainties deduced from the standard GOSIA analysis.

TABLE III. Diagonal matrix elements and quadrupole moments in $^{126,128}\text{Xe}$ determined in the present work. A comparison to results from PMMU shell-model calculations is presented. The experimental values are also compared with asymmetric rotor calculations (Q_s^{DF}), given that the sign of $Q(2_1^+)$ is negative.

^{126}Xe				
J_i^π	$\langle J_i^\pi E2 J_i^\pi \rangle_{\text{expt}}$ [eb]	Q_s^{expt} [eb]	Q_s^{PMMU} [eb]	Q_s^{DF} [eb]
2_1^+	-1.0 (2)	-0.76 (15)	-0.57	-0.52
4_1^+	-0.78 (16)	-0.59 (12)	-0.69	-0.30
2_2^+	+0.14 (9)	+0.11 (7)	+0.51	+0.52
^{128}Xe				
J_i^π	$\langle J_i^\pi E2 J_i^\pi \rangle_{\text{expt}}$ [eb]	Q_s^{expt} [eb]	Q_s^{PMMU} [eb]	Q_s^{DF} [eb]
2_1^+	-0.58 (-15 +12)	-0.44 (-12 +9)	-0.37	-0.49
4_1^+	-1.38 (13)	-1.04 (10)	-0.45	-0.28
2_2^+	+0.01 (-10 +9)	+0.008 (-0.08 +0.07)	+0.33	+0.49

IV. DISCUSSION

Besides the transition probability for the decay of the first excited state in ^{126}Xe , the $B(E2)$ values determined in the present work are in a reasonable agreement with previous measurements [1,8,9,13,37].

Although the experimental $B(E2; 2_1^+ \rightarrow 0_1^+) = 56 (5)$ W.u. for the decay of the 2_1^+ state in ^{126}Xe differs from the evaluated data in Refs. [28,31] [$B(E2) = 44 (4)$ W.u. in Ref. [28]], it fits well with recently performed measurements [36,38,39] reporting values of 56.5 (16) W.u. and 54.2 (+70 -30) W.u. A broad range of experimental results were reported for this transition probability over the years [37]. In a recent Coulomb excitation study [8] the value from the evaluation in Ref. [40] (which does not take into account the results presented in Ref. [39] and Ref. [36]) was used to set the absolute scale. The result obtained in the present work with the ^{196}Pt target dataset differs from that value.

In general, the $B(E2; 2_1^+ \rightarrow 0_1^+)$ values follow a smooth trend along the Xe isotopic chain [1]. They decrease with increasing the neutron number towards the shell closure at $N = 82$, pointing out well the collective properties in the midshell region. The $R_{4/2} \approx 2.5$, as well as the decay patterns of the lowest-lying states are consistent with the concept for γ softness and O(6) characteristics of $^{126,128}\text{Xe}$. Nevertheless, the relation to the O(6) dynamical symmetry was questioned based on the decay properties of some excited states [8,9].

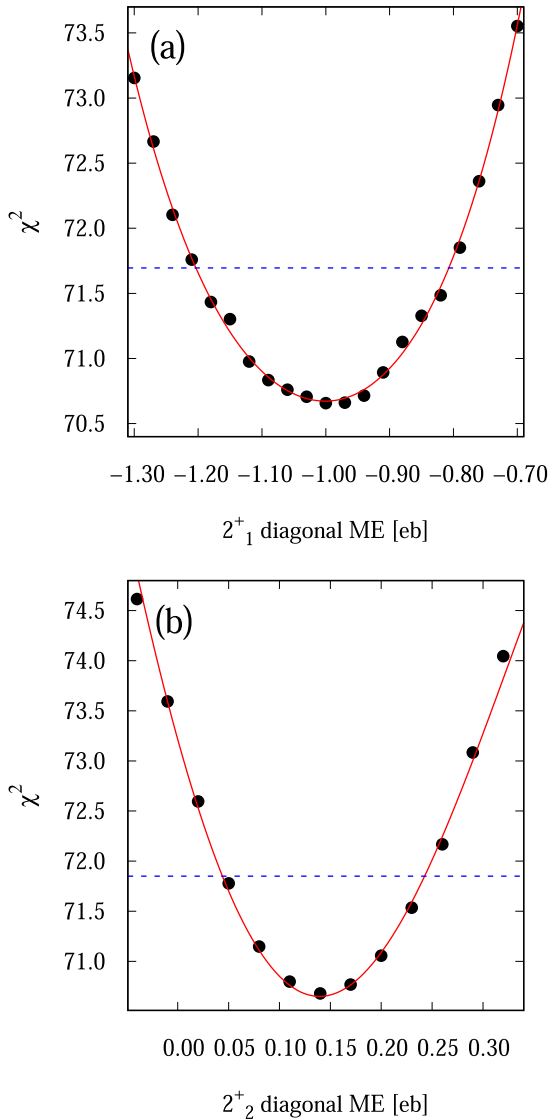


FIG. 5. Total χ^2 plotted as a function of the (a) $\langle 2_1^+ \parallel E2 \parallel 2_1^+ \rangle$ and (b) $\langle 2_2^+ \parallel E2 \parallel 2_2^+ \rangle$ diagonal matrix elements (ME) in ^{126}Xe measured in the current work. The uncertainties of the experimental values were determined on the basis of the $\chi^2 + 1$ criteria [33]. Fits of the experimental data points with a polynomial function are presented with continuous red lines in the plots while the $\chi^2 + 1$ values are shown with straight dashed blue lines.

The newly determined quadrupole moments of the first 2^+ states in $^{126,128}\text{Xe}$ also suggest deviations from the O(6) symmetry in the ground-state band of the nuclei. Their large magnitudes are in conflict with the O(6) limit, which implies vanishing quadrupole moments. The results are consistent in a systematic way with recently performed Coulomb excitation measurements in ^{130}Xe where a value of $Q(2_1^+) = -0.38 (+17 - 14)$ eb was determined [15].

A. Comparison with model predictions

The experimental quadrupole moments of the second excited 2^+ states are of significant interest since the measured

values are close to zero. These newly determined quadrupole moments in both nuclei are lower in magnitude compared with the measured $Q(2_1^+)$. This is also consistent in a systematic way with the $Q(2_2^+) = 0.1$ (1) eb value in ^{130}Xe [15]. Such a behavior seems to agree with a recent study concluding that the ground-band levels in ^{126}Xe may exhibit O(5) symmetry, while the excited bands have the characteristics of O(6) symmetry [41].

The measured $Q(2_1^+)$ are also reduced compared with a simple γ -rigid symmetric rotor model [$Q(2_1^+)_{\text{rot}} = -0.93$ eb for ^{126}Xe and $Q(2_1^+)_{\text{rot}} = -0.85$ eb for ^{128}Xe]. To study the possible triaxiality of the nuclei, $B(E2)$ values and quadrupole moments were calculated using the γ -rigid asymmetric rotor approach [2]. The triaxiality parameters γ were determined from the experimental strengths for the $2_2^+ \rightarrow 2_1^+$ and $2_1^+ \rightarrow 0_1^+$ transitions in $^{126,128}\text{Xe}$. In both cases the triaxiality parameters are similar ($\gamma \approx 26^\circ$). These values agree with an independent determination of the γ parameter from the excitation energies of the first 2^+ excited states in the nuclei. The ratios between the electromagnetic transition probabilities for the respective values of γ in both nuclei were deduced from the model. A normalization with respect to the experimental $\langle 2_1^+ \parallel E2 \parallel 0_1^+ \rangle$ transition matrix element in each nucleus was performed. A comparison to the measured values is presented in Tables II and III. The collective structure of $^{126,128}\text{Xe}$ was investigated in more detail by microscopic shell-model calculations. The model employs a realistic Hamiltonian (called PMMU) combining the pairing plus multipole terms with the monopole interaction obtained by the monopole based universal force [42], which has been proven to work well over a wide range of nuclei for describing nuclear properties such as energy spectra and electromagnetic transitions [43,44]. In the recent study of the neighboring ^{130}Xe isotope, the authors of Ref. [15] found that, for their shell-model description, unusually large effective charges were needed to reproduce the quadrupole transition strengths. That together with an overprediction of the excitation energies in Ref. [15] indicated that their model space between the shell gaps at $N, Z = 50$ and 82 is not large enough to describe the collective nature of this region. In contrast, our PMMU model adopts a much larger model space ($1g_{9/2}, 1g_{7/2}, 2d_{5/2}, 2d_{3/2}, 3s_{1/2}, 1h_{11/2}, 2f_{7/2}$) (referred to as *gdshf*). However, with such a large model space, a conventional shell-model calculation cannot be performed. To overcome this problem, an advanced many-body technique is required. In a recent development [45], Shimizu *et al.* proposed the Hartree-Fock-Bogoliubov plus generator coordinate method (HFB + gcm) to solve the shell model in a large model space. Briefly, it uses the HFB method to generalize a suitable mean field and applies the gcm calculation to obtain the wave functions by superimposing many configurations in the quadrupole-deformation plane. In this way, the effect of shape changes can be included. Furthermore, the HFB method makes it possible to visualize the nuclear shape through the plots of potential-energy surfaces. Hence, this is a powerful tool for nuclei of γ softness and can generally study shape evolution in heavy-mass regions as functions of particle number and spin. It has been shown [35] that the quadrupole interaction in the quasi-SU(3) partner orbits ($1g_{9/2}, 2d_{5/2}$) and

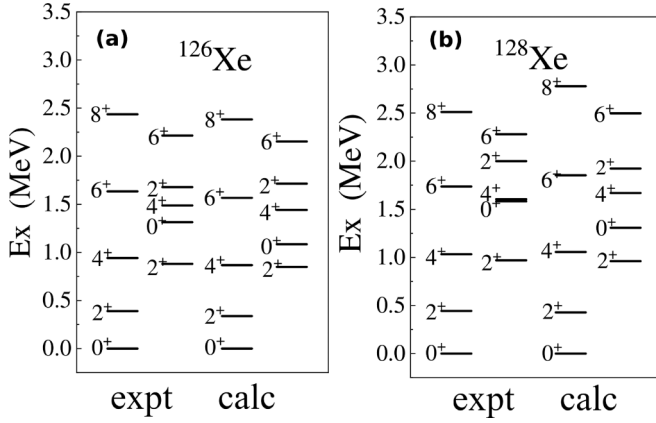


FIG. 6. Experimental energy levels (expt) for (a) ^{126}Xe and (b) ^{128}Xe compared with calculated energy levels within the PMMU shell model (calc). Not all of the states plotted in the figure were observed in the present experiment.

($1h_{11/2}, 2f_{7/2}$) across the $Z = 50$ and $N = 82$ shell gaps, respectively, are responsible for the observed large quadrupole collectivity.

We perform the PMMU shell-model calculation for ^{126}Xe and ^{128}Xe in the *gdshf* model space employing the same HFB + gcm code as in Ref. [46] and using the same parameters as in Ref. [35]. Figure 6 compares measured and calculated energy levels for ^{126}Xe and ^{128}Xe . For both nuclei, the calculations excellently reproduce the ground-state band as well as the sideband in the experiments built on the second

excited 2_2^+ state, while the first excited 0^+ state is calculated to be slightly lower than the experimental level. The calculated energy ratios, $R_{4/2} = 2.56$ and 2.46 for ^{126}Xe and ^{128}Xe , are in good agreement with the experimental ones, 2.42 and 2.33 , respectively. These $R_{4/2}$ ratios lie in the middle of the characteristic vibrational (2.0) and rotational (3.3) values and are consistent with the γ -soft (2.5) value. Therefore, the sideband may be understood in terms of a γ -vibration nature.

The calculated $B(E2)$ and Q_s values are compared with experimental data in Tables II and III, respectively, where the effective charges are taken as $e_p = 1.0e$ and $e_n = 0.4e$. A visual representation of the experimental and theoretical values is shown in Fig. 7. It is remarkable that the PMMU calculations reproduce well the small experimental $B(E2; 2_2^+ \rightarrow 0_1^+)$ for ^{126}Xe and ^{128}Xe . It should be noted that the γ -soft model predicts a small $B(E2)$ value for this transition, consistent with this result. In contrast, for models such as the DF which enforce γ rigidity and irrotational flow, a much larger $B(E2)$ value is predicted. We note that, when the inertial tensor is treated independently [47], a rigid rotor can also satisfy this weak $B(E2)$.

However, as listed in Table III, the experimental Q_s values of 0.11 (7) eb and 0.008 ($-0.08 + 0.07$) eb for the second excited 2_2^+ states are significantly smaller than the theoretical values, 0.51 and 0.33 eb, respectively. This situation is similar to the recent ^{130}Xe data [15]. In ^{130}Xe , all theoretical calculations predict a large positive Q_s value for the second 2_2^+ state, as discussed by Morrison *et al.* [15]. In their calculations, it is notable that the absolute Q_s value is almost the same as that of the first 2_1^+ state, while it has the opposite sign. Thus, it seems

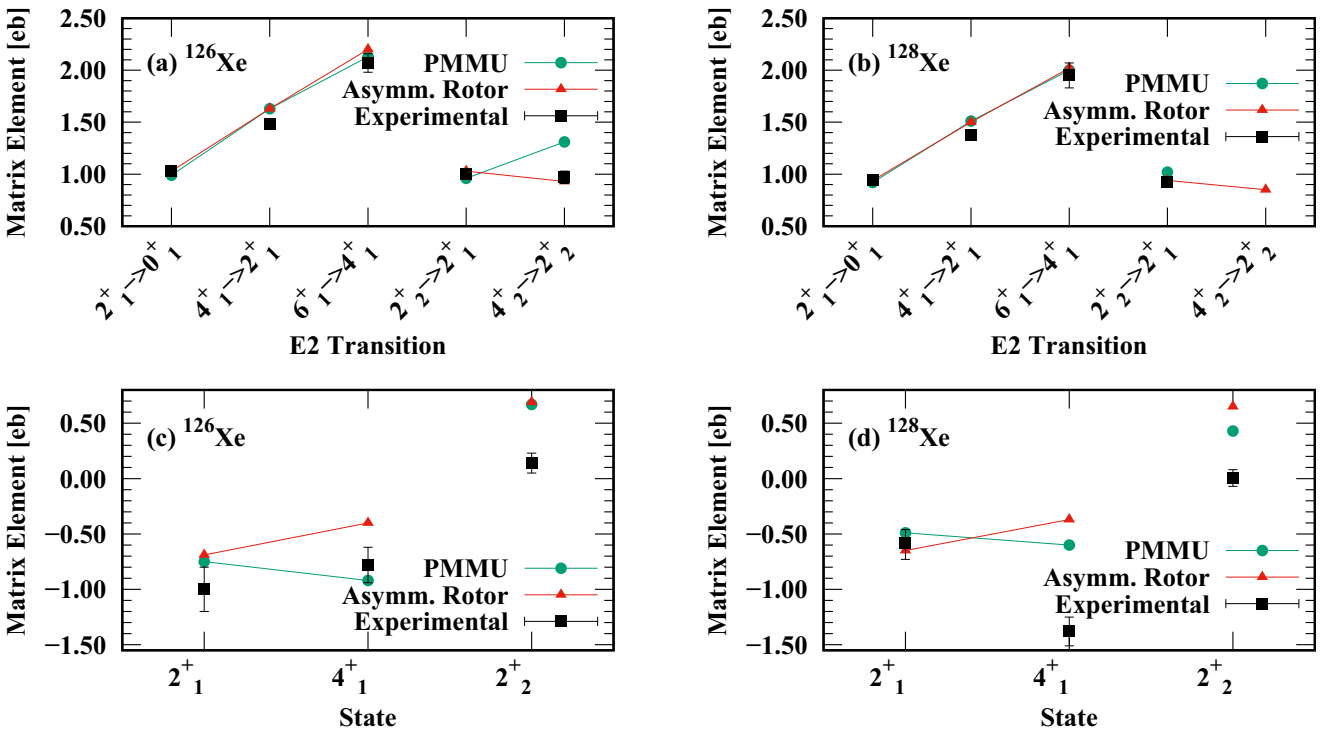


FIG. 7. A comparison between experimental values (black squares) and calculations within the PMMU shell model (green circles) and the asymmetric rotor model (red triangles) for (a) transition matrix elements in ^{126}Xe , (b) transition matrix elements in ^{128}Xe , (c) diagonal matrix elements in ^{126}Xe , (d) diagonal matrix elements in ^{128}Xe .

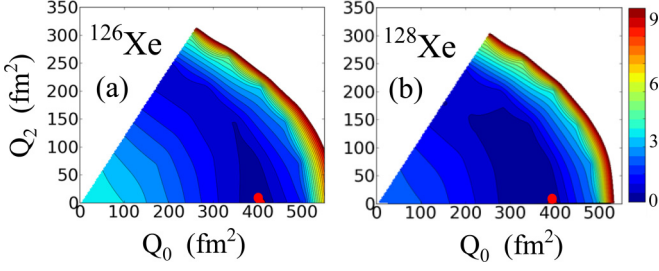


FIG. 8. Potential-energy surfaces (PES) for ^{126}Xe and ^{128}Xe .

to be difficult for the current shell models to obtain the small Q_s value for the second excited 2_2^+ state in ^{126}Xe and ^{128}Xe as well as in the ^{130}Xe case.

Experimental data for $Q(2_2^+)$ along the nuclear chart are sparse and often the uncertainties of the measured values are large [48]. Although some experimental results in nuclei with well-defined and observed γ bands follow the $Q(2_2^+) \approx -Q(2_1^+)$ dependence, a general statement for the uniqueness of the situation in the Xe isotopes is difficult.

An interpretation for the experimentally determined nearly vanishing electric quadrupole moment, Q_s in 2_2^+ , is currently challenging. To learn more about the nature of the studied nuclei, we examine the potential-energy surface (PES) obtained by the constraint HFB method from our PMMU model. The PES plots as functions of quadrupole moments Q_0 and Q_2 for ^{126}Xe and ^{128}Xe are shown in Fig. 8. Both plots suggest extremely soft energy surfaces for a wide area in the parameter plane so that it is impossible to talk meaningfully about shape for these two nuclei. With such kind of potential surface it is not difficult to imagine that a perturbation (such as rotation) can easily drive the nucleus moving in the Q_0 - Q_2 plane. In other words, for a nucleus with no well-defined shape there can be rich possibilities to develop shape(s) including unusual ones when it gets excited. This seems to be what we have encountered in the present examples.

B. Model-independent determination of quadrupole shape parameters

The new experimental results were used to extract collective parameters in a model-independent way by applying sum rules as outlined in Refs. [17,23,49,50]. Zero-coupled products of spherical tensors are rotationally invariant. The expectation values of such products for the electric-quadrupole operators can be expressed in terms of the model-independent parameters Q and δ . The first two rotational invariants for a given state s are

$$\langle s | \widehat{Q}^2 | s \rangle = \sqrt{5} \langle s | [\widehat{E}2 \times \widehat{E}2]_0 | s \rangle \quad (1)$$

and

$$\langle s | Q^3 \cos 3\delta | s \rangle = \sqrt{\frac{35}{2}} \langle s | \{ [\widehat{E}2 \times \widehat{E}2]_2 \times \widehat{E}2 \}_0 | s \rangle. \quad (2)$$

Using the short notation for matrix elements $M_{if} = \langle i | \widehat{E}2 | f \rangle$, intermediate state (t, u) expansions can be written

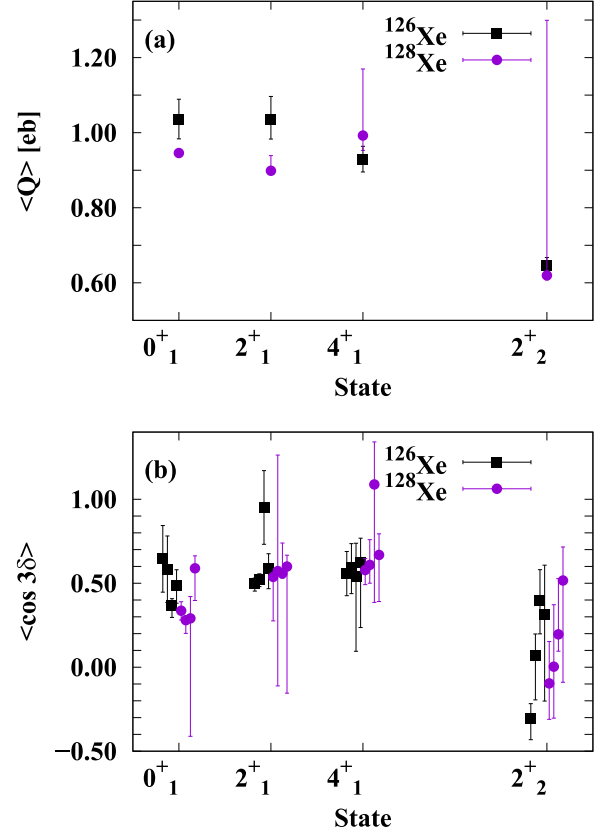


FIG. 9. Centroids of the (a) magnitude and (b) asymmetry of the intrinsic frame $E2$ properties for states in $^{126,128}\text{Xe}$, determined from the experimental matrix elements measured in the present work. The four different points for the asymmetry of each state in $^{126,128}\text{Xe}$ correspond to values derived from four different calculated rotational invariants, along with their uncertainties.

as

$$\langle s | [\widehat{E}2 \times \widehat{E}2]_0 | s \rangle = \frac{(-1)^{2I_s}}{\sqrt{(2I_s + 1)}} \sum_t M_{st} M_{ts} \left\{ \begin{matrix} 2 & 2 & 0 \\ I_s & I_s & I_t \end{matrix} \right\} \quad (3)$$

and

$$\begin{aligned} \langle s | \{ [\widehat{E}2 \times \widehat{E}2]_2 \times \widehat{E}2 \}_0 | s \rangle \\ = \frac{(-1)^{2I_s}}{(2I_s + 1)} \sum_{tu} M_{su} M_{ut} M_{ts} \left\{ \begin{matrix} 2 & 2 & 2 \\ I_s & I_t & I_u \end{matrix} \right\}, \end{aligned} \quad (4)$$

where $\{ \dots \}$ represent the Wigner $6j$ symbols. Higher-order invariants can be constructed using the different intermediate-spin couplings and summation over different sets of data. This procedure allows for a self-consistency verification of the invariants. A more detailed insight on different couplings can be found in Ref. [23].

The Q and $\cos 3\delta$ parameters for states in $^{126,128}\text{Xe}$ were investigated with the present sets of experimental data. The values obtained for the 0_1^+ , 2_1^+ , 4_1^+ , and 2_2^+ states in $^{126,128}\text{Xe}$ are presented in Fig. 9. The magnitudes of Q show consistent results for the quadrupole deformation within the ground-state bands. For the 2_2^+ states, the smaller Q values indicate a possible incomplete summation or a less deformed shape.

The asymmetry parameters $\cos 3\delta$ were determined using different invariants, allowing to check their completeness and convergence. The results suggest similar triaxiality in the ground-state bands of both nuclei. Although some of the summations lead to high uncertainty of particular $\cos 3\delta$ values, the calculations show that, in general, $\cos 3\delta \approx 0.5$ in the ground-state bands in $^{126,128}\text{Xe}$. The asymmetry parameters could not be clearly determined for the 2_2^+ states in both nuclei. It is possible that there is missing strength from higher-lying excited states in the present dataset due to the nonobservation of the transitions. Thus, the summation within the measured matrix elements datasets for the second excited 2^+ states may be incomplete.

V. SUMMARY

The electromagnetic properties of $^{126,128}\text{Xe}$ were studied in subbarrier Coulomb excitation measurements performed at ReA3 using the JANUS setup. Results for transition probabilities in both nuclei are in a reasonable agreement with previously known values from the literature. The newly measured quadrupole moments of low-lying excited states suggest a prolate deformation of both nuclei and a deviation from the $O(6)$ dynamical symmetry in the ground-state bands.

The schematic rigid- γ rotor model and the microscopic shell-model calculations were performed for the

$^{126,128}\text{Xe}$ isotopes. The experimental transition probabilities and quadrupole moments are in general in a reasonable agreement with the theoretical results. However, the calculations fail to reproduce the experimentally determined electric-quadrupole moment of the second 2^+ states in both nuclei, resulting in a challenge to understand the unusual structure of the γ bands in these nuclei.

ACKNOWLEDGMENTS

This work was performed under the auspices of the U.S. Department of Energy by Lawrence Livermore National Laboratory under Contract DE-AC52-07NA27344. The work was supported by US DOE Contract No. 89233218CNA000001, and by the U.S. DOE, Office of Science, Office of Nuclear Physics, under Grant No. DE-SC0020451, the US National Science Foundation (NSF) under Grant No. PHY-1565546, and by the DOE National Nuclear Security Administration through the Nuclear Science and Security Consortium, under Award No. DE-NA0003180. Y.S. was supported by the National Natural Science Foundation of China under Contract No. U1932206. K.K. and N.S. were supported by the Multidisciplinary Cooperative Research Program in CCS, University of Tsukuba (xg18i035, wo22i002). J.H. acknowledges support at the University of Surrey under UKRI Future Leaders Fellowship MR/T022264/1.

-
- [1] NNDC data base, www.nndc.bnl.gov.
- [2] A. S. Davydov and G. F. Filippov, *Nucl. Phys.* **8**, 237 (1958).
- [3] L. Wilets and M. Jean, *Phys. Rev.* **102**, 788 (1956).
- [4] T. Otsuka and M. Sugita, *Phys. Rev. Lett.* **59**, 1541 (1987).
- [5] N. V. Zamfir and R. F. Casten, *Phys. Lett. B* **260**, 265 (1991).
- [6] G. H. Bhat, W. A. Dar, J. A. Sheikh, and Y. Sun, *Phys. Rev. C* **89**, 014328 (2014).
- [7] R. F. Casten, *Nuclear Structure from a Simple Perspective* (Oxford University Press, New York, 1990).
- [8] L. Coquard, G. Rainovski, N. Pietralla, T. Ahn, L. Bettermann, M. P. Carpenter, R. V. F. Janssens, J. Leske, C. J. Lister, O. Möller, T. Möller, W. Rother, V. Werner, and S. Zhu, *Phys. Rev. C* **83**, 044318 (2011).
- [9] L. Coquard, N. Pietralla, T. Ahn, G. Rainovski, L. Bettermann, M. P. Carpenter, R. V. F. Janssens, J. Leske, C. J. Lister, O. Möller, W. Rother, V. Werner, and S. Zhu, *Phys. Rev. C* **80**, 061304(R) (2009).
- [10] R. M. Clark, M. Cromaz, M. A. Deleplanque, M. Descovich, R. M. Diamond, P. Fallon, I. Y. Lee, A. O. Macchiavelli, H. Mahmud, E. Rodriguez-Vieitez, F. S. Stephens, and D. Ward, *Phys. Rev. C* **69**, 064322 (2004).
- [11] T. Otsuka, *Hyperfine Interact.* **78**, 19 (1993).
- [12] G. Puddu, O. Scholten, and T. Otsuka, *Nucl. Phys. A* **348**, 109 (1980).
- [13] J. Srebrny, T. Czosnyka, W. Karczmarczyk, P. Napiorkowski, Ch. Droste, H.-J. Wollersheim, H. Emling, H. Grein, R. Kulesa, D. Cline, and C. Fahlander, *Nucl. Phys. A* **557**, 663 (1993).
- [14] C. Fransen, A. Dewald, T. Baumann, D. Bazin, A. Blazhev, B. A. Brown, A. Chester, A. Gade, T. Glasmacher, P. T. Greenlees, M. Hackstein, S. Harissopulos, U. Jakobsson, J. Jolie, P. M. Jones, R. Julin, S. Juutinen, S. Ketelhut, T. Konstantinopoulos, A. Lagoyannis *et al.*, *J. Phys.: Conf. Ser.* **205**, 012043 (2010).
- [15] L. Morrison, K. Hadyńska-Klęk, Z. Podolyák, D. T. Doherty, L. P. Gaffney, L. Kaya, L. Próchniak, J. Samorajczyk-Pyšk, J. Srebrny, T. Berry, A. Boukhari, M. Brunet, R. Canavan, R. Catherall, S. J. Colosimo, J. G. Cubiss, H. De Witte, Ch. Fransen, E. Giannopoulos, H. Hess, T. Kröll, N. Lalovic, B. Marsh, Y. M. Palenzuela, P. J. Napiorkowski, G. O'Neill, J. Pakarinen, J. P. Ramos, P. Reiter, J. A. Rodriguez, D. Rosiak, S. Rothe, M. Rudigier, M. Siciliano, J. Snäll, P. Spagnoletti, S. Thiel, N. Warr, F. Wenander, R. Zidarova, and M. Zielinska, *Phys. Rev. C* **102**, 054304 (2020).
- [16] A. Lapiere, G. Bollen, D. Crisp, S. W. Krause, L. E. Linhardt, K. Lund, S. Nash, R. Rencsok, R. Ringle, S. Schwarz, M. Steiner, C. Sumithrarachchi, T. Summers, A. C. C. Villari, S. J. Williams, and Q. Zhao, *Phys. Rev. Accel. Beams* **21**, 053401 (2018).
- [17] D. Cline, *Annu. Rev. Nucl. Part. Sci.* **36**, 683 (1986).
- [18] E. Lunderberg, J. Belarge, P. C. Bender, B. Bucher, D. Cline, B. Elman, A. Gade, S. N. Liddick, B. Longfellow, C. Prokop, D. Weisshaar, and C. Y. Wu, *Nucl. Instrum. Methods Phys. Res., Sect. A* **885**, 30 (2018).
- [19] W. F. Mueller, J. A. Church, T. Glasmacher, D. Gutknecht, G. Hackman, P. G. Hansen, Z. Hu, K. L. Miller, and P. Quirin, *Nucl. Instrum. Methods Phys. Res., Sect. A* **466**, 492 (2001).
- [20] D. Rhodes, B. A. Brown, A. Gade, S. Biswas, A. Chester, P. Farris, J. Henderson, A. Hill, J. Li, F. Nowacki, E. Rubino, D. Weisshaar, and C. Y. Wu, *Phys. Rev. C* **105**, 024325 (2022).

- [21] P. C. Bender, <https://github.com/pcbend/grutinizer>.
- [22] R. Brun and Fons Rademakers, Proceedings AIHENP'96 Workshop, Lausanne(1996); *Nucl. Inst. Meth. Phys. Res. A* **389**, 81 (1997).
- [23] T. Czosnyka, D. Cline, and C. Y. Wu, *Bull. Am. Phys. Soc.* **28**, 745 (1983).
- [24] D. Cline, T. Czosnyka, A. B. Hayes, P. Napiorkowski, N. Warr, and C. Y. Wu, Gosia manual, Version: May 10, 2012, http://www.pas.rochester.edu/~cline/Gosia/Gosia_Manual_20120510.pdf.
- [25] L. P. Gaffney, <https://github.com/lpgaff/chisqsurface>.
- [26] J. Henderson, <https://github.com/jhenderson88/GOSIAFitter>.
- [27] M. Zielińska, L. P. Gaffney, K. Wrzosek-Lipska, E. Clément, T. Grahn, N. Kesteloot, P. Napiorkowski, J. Pakarinen, P. Van Duppen, and N. Warr, *Eur. Phys. J. A* **52**, 99 (2016).
- [28] H. Iimura, J. Katakura, and S. Ohya, *Nucl. Data Sheets* **180**, 1 (2022).
- [29] Z. Elekes and J. Timar, *Nucl. Data Sheets* **129**, 191 (2015).
- [30] W. Rother, A. Dewald, G. Pascovici, C. Fransen, G. Frießner, M. Hackstein, G. Ilie, H. Iwasaki, J. Jolie, B. Melon, P. Petkov, M. Pfeiffer, Th. Pissulla, K.-O. Zell, U. Jakobsson, R. Julin, P. Jones, S. Ketelhut, P. Nieminen, P. Peura *et al.*, *Nucl. Instrum. Methods Phys. Res., Sect. A* **654**, 196 (2011).
- [31] J. Katakura and K. Kitao, *Nucl. Data Sheets* **97**, 765 (2002).
- [32] T. Konstantinopoulos, A. Lagoyannis, S. Harissopoulos, A. Dewald, C. Fransen, G. Frießner, M. Hackstein, J. Jolie, G. Pascovici, Th. Pissulla, W. Rother, K.-O. Zell, G. Ilie, H. Iwasaki, B. Melon, U. Jakobsson, R. Julin, P. Jones, S. Ketelhut, P. Nieminen *et al.*, *HNPS Adv. Nucl. Phys.* **18**, 7 (2010).
- [33] D. Cline and P. M. S. Lesser, *Nucl. Instrum. Methods* **82**, 291 (1970).
- [34] C. Y. Wu, D. Cline, T. Czosnyka, A. Backlin, C. Baktash, R. M. Diamond, G. D. Dracoulis, L. Hasselgren, H. Kluge, B. Kotlinski, J. R. Leigh, J. O. Newton, W. R. Phillips, S. H. Sie, J. Srebrny, and F. S. Stephens, *Nucl. Phys. A* **607**, 178 (1996).
- [35] K. Kaneko, N. Shimizu, T. Mizusaki, and Y. Sun, *Phys. Rev. C* **103**, L021301 (2021).
- [36] W. F. Mueller, M. P. Carpenter, J. A. Church, D. C. Dinca, A. Gade, T. Glasmacher, D. T. Henderson, Z. Hu, R. V. F. Janssens, A. F. Lisetskiy, C. J. Lister, E. F. Moore, T. O. Pennington, B. C. Perry, I. Wiedenhöver, K. L. Yurkewicz, V. G. Zelevinsky, and H. Zwahlen, *Phys. Rev. C* **73**, 014316 (2006).
- [37] B. Pritychenko, M. Birch, B. Singh, and M. Horoi, *At. Data Nucl. Data Tables* **107**, 1 (2016).
- [38] O. Stuch, Ph.D. thesis, University of Cologne, 1997 (unpublished).
- [39] A. Gade, I. Wiedenhover, J. Gableske, A. Gelberg, H. Meise, N. Pietralla, and P. von Brentano, *Nucl. Phys. A* **665**, 268 (2000).
- [40] S. Raman, C. W. Nestor, and P. Tikkanen, *At. Data Nucl. Data Tables* **78**, 1 (2001).
- [41] J. B. Gupta and J. H. Hamilton, *Phys. Rev. C* **104**, 054325 (2021).
- [42] T. Otsuka, T. Suzuki, M. Honma, Y. Utsuno, N. Tsunoda, K. Tsukiyama, and M. Hjorth-Jensen, *Phys. Rev. Lett.* **104**, 012501 (2010).
- [43] K. Kaneko, T. Mizusaki, Y. Sun, and S. Tazaki, *Phys. Rev. C* **89**, 011302(R) (2014).
- [44] K. Kaneko, T. Mizusaki, Y. Sun, and S. Tazaki, *Phys. Rev. C* **92**, 044331 (2015).
- [45] N. Shimizu, T. Mizusaki, K. Kaneko, and Y. Tsunoda, *Phys. Rev. C* **103**, 064302 (2021).
- [46] N. Shimizu, HFB + gcm code (2019) (unpublished).
- [47] J. M. Allmond, J. L. Wood, and W. D. Kulp, *Phys. Rev. C* **81**, 051305(R) (2010).
- [48] N. J. Stone, *At. Data Nucl. Data Tables* **111-112**, 1 (2016).
- [49] K. Kumar, *Phys. Rev. Lett.* **28**, 249 (1972).
- [50] J. Henderson, *Phys. Rev. C* **102**, 054306 (2020).